arXiv:1902.04914v1 [cond-mat.mtrl-sci] 13 Feb 2019

Mode I crack tip fields: strain gradient plasticity theory versus J2 flow theory

Emilio Martínez-Pañeda[a,*], Norman A. Fleck[a]

[a]*Department of Engineering, Cambridge University, CB2 1PZ Cambridge, UK*

Abstract

The mode I crack tip asymptotic response of a solid characterised by strain gradient plasticity is investigated. It is found that elastic strains dominate plastic strains near the crack tip, and thus the Cauchy stress and the strain state are given asymptotically by the elastic K-field. This crack tip elastic zone is embedded within an annular elasto-plastic zone. This feature is predicted by both a crack tip asymptotic analysis and a finite element computation. When small scale yielding applies, three distinct regimes exist: an outer elastic K field, an intermediate elasto-plastic field, and an inner elastic K field. The inner elastic core significantly influences the crack opening profile. Crack tip plasticity is suppressed when the material length scale ℓ of the gradient theory is on the order of the plastic zone size estimation, as dictated by the remote stress intensity factor. A generalized J-integral for strain gradient plasticity is stated and used to characterise the asymptotic response ahead of a short crack. Finite element analysis of a cracked three

---

*Corresponding author.
Email address: `mail@empaneda.com` (Emilio Martínez-Pañeda)

point bend specimen reveals that the crack tip elastic zone persists in the presence of bulk plasticity and an outer J-field.

1. Introduction

Strain gradient plasticity is increasingly used in fracture analyses to predict the stress elevation that accompanies gradients of plastic strain, see, for example, (Wei and Hutchinson, 1997; Jiang et al., 2001; Komaragiri et al., 2008; Nielsen et al., 2012; Martínez-Pañeda et al., 2017b) and references therein. Gradients of plastic strain are associated with lattice curvature and geometrically necessary dislocations (Ashby, 1970), and the increased dislocation density promotes strengthening. Flow stress elevation in the presence of plastic strain gradients has been observed in a wide range of mechanical tests on micro-sized specimens. Representative examples are indentation (Poole et al., 1996; Nix and Gao, 1998), torsion (Fleck et al., 1994), and bending (Stölken and Evans, 1998). These experiments typically predict a 3-fold increase in the effective flow stress by reducing the size of the specimen (*smaller is stronger*). Isotropic, strain gradient plasticity theories have been developed to capture this size effect. The pivotal step in constructing these phenomenological models is to write the plastic work increment in terms of both the plastic strain and plastic strain gradient, thereby introducing a length scale in the material description (Aifantis, 1984; Gao et al., 1999; Fleck and Hutchinson, 2001; Gurtin and Anand, 2005). Work-conjugate stress

2

quantities for plastic strain and plastic strain gradient follow immediately.

The crack tip stress elevation, as predicted by strain gradient plasticity theory relative to conventional plasticity theory, plays a fundamental role in the modelling of numerous damage mechanisms (Martínez-Pañeda and Betegón, 2015; Martínez-Pañeda and Niordson, 2016). Examples include fatigue (Brinckmann and Siegmund 2008; Pribe et al., 2019), notch mechanics (Martínez-Pañeda et al., 2017a), microvoid cracking (Tvergaard and Niordson, 2008), and hydrogen embrittlement (Martínez-Pañeda et al., 2016a,b).

In the present study, we examine the mode I crack tip field according to strain gradient plasticity theory (Gudmundson, 2004; Fleck and Willis, 2009). Previous crack tip asymptotic studies considered earlier gradient plasticity classes, such as couple-stress theories without stretch gradients (Huang et al., 1997; Xia and Hutchinson, 1996) or models involving the gradients of elastic strains (Chen et al., 1999). For such theories, plastic strains dominate elastic strains near the crack tip and the asymptotic nature of the crack tip field can be obtained by neglecting elasticity. This is analogous to the HRR (Hutchinson, 1968; Rice and Rosengren, 1968) analysis for a conventional elasto-plastic solid.

We shall show in the present study that the crack tip field for Gudmundson-type strain gradient theories is of a different nature, such that the asymptotic crack tip field comprises both elastic and plastic straining, and it is not possible to simplify the crack tip asymptotic state by neglecting elastic strains.

3

Instead, the elastic strain ε_{ij}^e scales as $r^{-1/2}$ with distance r from the crack tip, whereas the plastic strain tensor $\underset{\sim}{\varepsilon}^p(\underline{x})$ is of the form

$$\underset{\sim}{\varepsilon}^p(\underline{x}) = \underset{\sim}{\varepsilon}^p(0) + \underset{\sim}{\tilde{\varepsilon}}^p(\underline{x}) + \cdots \tag{1}$$

The leading order term $\underset{\sim}{\varepsilon}^p(0)$ has a finite value independent of $\underline{x}$. The next term in the series, $\underset{\sim}{\tilde{\varepsilon}}^p(\underline{x})$, scales as $r^{3/2}$ where $r = |x|$ is the polar coordinate from the crack tip, and $\underset{\sim}{\tilde{\varepsilon}}^p(\underline{x})$ also depends upon the polar coordinate θ. Thus, we can write ε_{ij}^p in polar coordinates as,

$$- \varepsilon_{rr}^p = \varepsilon_{\theta\theta}^p = A\cos(2\theta) + r^{3/2}f(\theta) + \cdots \tag{2}$$

$$\varepsilon_{r\theta}^p = A\sin(2\theta) + r^{3/2}g(\theta) + \cdots \tag{3}$$

Later, in the paper, we shall obtain explicit expressions for the angular functions $f(\theta)$ and $g(\theta)$. Thus, the elastic strain is more singular than the plastic strain and the Cauchy stress $\sigma_{ij}(r,\theta)$ is given by the usual elastic K-field in the vicinity of the crack tip.

The following simple argument supports the finding that the crack tip is surrounded by an elastic K-field in an elastic-plastic strain gradient solid. Introduce a generalized effective plastic strain $\tilde{E}^p$ such that

$$\left(\tilde{E}^p\right)^2 = \frac{2}{3}\varepsilon_{ij}^p\varepsilon_{ij}^p + \ell^2\varepsilon_{ij,k}^p\varepsilon_{ij,k}^p \tag{4}$$

in terms of a material length scale ℓ; the comma subscript $()_{,k}$ denotes spatial differentiation with respect to the coordinate x_k in the usual manner. Consider the case of a deformation theory solid, and assume that the plastic strain energy density w^p scales as $\tilde{E}^{p^{(N+1)}}$ in terms of a strain hardening

4

exponent N (where $0 \leq N \leq 1$). We proceed to show that the elastic strain must dominate the plastic strain. To do so, we shall explore the consequences of assuming that the plastic strain dominates the elastic strain near the crack tip. Then, w^p must scale as J/r in order for the energy release rate for crack advance to be finite at the crack tip. Consequently, $\tilde{E}^p$ and $\ell \varepsilon^p_{ij,k}$ scale as $r^{-1/(N+1)}$ and ε^p_{ij} scales as $r^{N/(N+1)}$. We conclude that ε^p_{ij} tends to zero as the crack tip is approached. If the elastic strain is dominated by the plastic strain then this implies that ε^e_{ij} tends to zero at a faster rate than $r^{N/(N+1)}$, and the crack tip will have a strain and a stress concentration of zero. This is implausible on physical grounds. We conclude that the elastic strain field must dominate the plastic strain field at the crack tip, and the Cauchy stress and elastic strain are given by the usual elastic K-field.

2. Strain Gradient Plasticity

We idealise strain gradient effects by means of the Gudmundson (2004) higher order gradient plasticity model, see also Fleck and Willis (2009). A brief summary of the constitutive and field equations for a flow theory version of strain gradient plasticity is now presented.

2.1. Variational principles and balance equations

The primal kinematic variables are the velocity $\dot{u}_i$ and the plastic strain rate $\dot{\varepsilon}^p_{ij}$. Upon adopting a small strain formulation, the total strain rate reads

$$\dot{\varepsilon}_{ij} = \frac{1}{2} \left(\dot{u}_{i,j} + \dot{u}_{j,i} \right) \tag{5}$$

and is decomposed additively into elastic and plastic parts,

$$\dot{\varepsilon}_{ij} = \dot{\varepsilon}^e_{ij} + \dot{\varepsilon}^p_{ij} \tag{6}$$

5

Write the internal work within a volume V as

$$\delta W = \int_V \left(\sigma_{ij} \delta \varepsilon_{ij}^e + q_{ij} \delta \varepsilon_{ij}^p + \tau_{ijk} \delta \varepsilon_{ij,k}^p \right) dV \tag{7}$$

where σ_{ij} denotes the Cauchy stress, q_{ij} the so-called micro-stress tensor (work-conjugate to the plastic strain ε_{ij}^p) and τ_{ijk} is the higher order stress tensor (work-conjugate to the plastic strain gradient $\varepsilon_{ij,k}^p$). The volume V is contained within a surface S of unit outward normal n_i. Now make use of Gauss' divergence theorem to re-express δW as the external work on the surface S,

$$\delta W = \int_S \left(\sigma_{ij} n_j \delta u_i + \tau_{ijk} n_k \delta \varepsilon_{ij}^p \right) dS \tag{8}$$

to obtain the following equilibrium equations within V:

$$\sigma_{ij,j} = 0$$

$$s_{ij} = q_{ij} - \tau_{ijk,k} \tag{9}$$

Here, s_{ij} is the deviatoric part of the Cauchy stress such that $s_{ij} = \sigma_{ij} - \delta_{ij} \sigma_{kk}/3$. Equations (7) and (8) constitute the Principle of Virtual Work,

$$\int_V \left(\sigma_{ij} \delta \varepsilon_{ij}^e + q_{ij} \delta \varepsilon_{ij}^p + \tau_{ijk} \delta \varepsilon_{ij,k}^p \right) dV = \int_S \left(T_i \delta u_i + t_{ij} \delta \varepsilon_{ij}^p \right) dS \tag{10}$$

where $T_i = \sigma_{ij} n_j$ and $t_{ij} = \tau_{ijk} n_k$ denote the conventional and higher order tractions, respectively.

2.2. Constitutive laws

The elastic strain ε_{ij}^e gives rise to an elastic strain energy density,

$$w^e = \frac{1}{2} \varepsilon_{ij}^e C_{ijkl} \varepsilon_{kl}^e \tag{11}$$

where $C_{ijkl} = C_{klij}$ is the isotropic elastic stiffness tensor, given in terms of Young's modulus E and Poisson's ratio ν. We identify the elastic work increment $\sigma_{ij}\delta\varepsilon_{ij}^e$ with δw^e such that

$$\sigma_{ij} = \frac{\partial w^e}{\partial\varepsilon_{ij}^e} = C_{ijkl}\varepsilon_{kl}^e \tag{12}$$

The stresses (q_{ij}, τ_{ijk}) are taken to be dissipative in nature and we assume that the plastic work rate $\dot{w}^p$ reads,

$$q_{ij}\delta\dot{\varepsilon}_{ij}^p + \tau_{ijk}\delta\dot{\varepsilon}_{ij,k}^p = \delta\dot{w}^p \tag{13}$$

where $\dot{w}^p(\dot{E}^p)$ is given in terms of a combined effective plastic strain rate,

$$\dot{E}^p = \left(\frac{2}{3}\dot{\varepsilon}_{ij}^p\dot{\varepsilon}_{ij}^p + \ell^2\dot{\varepsilon}_{ij,k}^p\dot{\varepsilon}_{ij,k}^p\right)^{1/2} \tag{14}$$

thereby introducing a material length scale ℓ. The use of (13) implies immediately that

$$q_{ij} = \frac{\partial\dot{w}^p}{\partial\dot{\varepsilon}_{ij}^p} = \frac{\partial\dot{w}^p}{\partial\dot{E}^p}\frac{\partial\dot{E}^p}{\partial\dot{\varepsilon}_{ij}^p} \tag{15}$$

and

$$\tau_{ijk} = \frac{\partial\dot{w}^p}{\partial\dot{\varepsilon}_{ij,k}^p} = \frac{\partial\dot{w}^p}{\partial\dot{E}^p}\frac{\partial\dot{E}^p}{\partial\dot{\varepsilon}_{ij,k}^p} \tag{16}$$

Upon introducing an overall effective stress $\Sigma = \partial\dot{w}^p/\partial\dot{E}^p$, these expressions reduce to

$$q_{ij} = \frac{2}{3}\frac{\Sigma}{\dot{E}^p}\dot{\varepsilon}_{ij}^p \quad \text{and} \quad \tau_{ijk} = \frac{\Sigma}{\dot{E}^p}\ell^2\dot{\varepsilon}_{ij,k}^p \tag{17}$$

Note that Σ is work conjugate to $\dot{E}^p$, such that it satisfies

$$\Sigma\dot{E}^p = q_{ij}\dot{\varepsilon}_{ij}^p + \tau_{ijk}\dot{\varepsilon}_{ij,k}^p \tag{18}$$

and, upon making use of (14) and (17) we obtain the relation

$$\Sigma = \left(\frac{3}{2}q_{ij}q_{ij} + \ell^{-2}\tau_{ijk}\tau_{ijk}\right)^{1/2} \tag{19}$$

7

3. Asymptotic analysis of crack tip fields

3.1. Deformation theory solid

We begin our study by conducting an asymptotic analysis of the stress and strain state at the crack tip. As already discussed in the introduction, consider a deformation theory solid such that the strain energy density $w\left(\varepsilon_{ij}^e,\ \varepsilon_{ij}^p,\ \varepsilon_{ij,k}^p\right)$ is decomposed into an elastic part w^e and a plastic part w^p,

$$w\left(\varepsilon_{ij}^e,\ \varepsilon_{ij}^p,\ \varepsilon_{ij,k}^p\right) = w^e\left(\varepsilon_{ij}^e\right) + w^p\left(\varepsilon_{ij}^p,\ \varepsilon_{ij,k}^p\right) \tag{20}$$

The elastic contribution is stated explicitly by (11). For the deformation theory solid the effective strain quantity $\tilde{E}^p$ has already been introduced by (4). The dissipation potential w^p is taken to be a power law function of $\tilde{E}^p$

$$w^p\left(\tilde{E}^p\right) = \frac{\sigma_Y \varepsilon_Y}{N+1}\left(\frac{\tilde{E}^p}{\varepsilon_Y}\right)^{N+1} \tag{21}$$

in terms of a reference value of strength σ_Y, yield strain $\varepsilon_Y = \sigma_Y/E$ and hardening index N (where $0 \le N \le 1$). Upon writing the dissipation increment δw^p as

$$\delta w^p = q_{ij}\delta\varepsilon_{ij}^p + \tau_{ijk}\delta\varepsilon_{ij,k}^p \tag{22}$$

and upon introducing the notation $\Sigma = \partial w^p/\partial\tilde{E}^p$, we have

$$q_{ij} = \frac{\partial w^p}{\partial\varepsilon_{ij}^p} = \Sigma\frac{\partial\tilde{E}^p}{\partial\varepsilon_{ij}^p} = \frac{2}{3}\frac{\Sigma}{\tilde{E}^p}\varepsilon_{ij}^p \tag{23}$$

$$\tau_{ijk} = \frac{\partial w^p}{\partial\varepsilon_{ij,k}^p} = \Sigma\frac{\partial\tilde{E}^p}{\partial\varepsilon_{ij,k}^p} = \ell^2\frac{\Sigma}{\tilde{E}^p}\varepsilon_{ij,k}^p \tag{24}$$

We note in passing that substitution of (23)-(24) into (4) recovers (19), and the relation between Σ and $\tilde{E}^p$ is of power law type, such that

$$\Sigma = \frac{\partial w^p}{\partial\tilde{E}^p} = \sigma_Y\left(\frac{\tilde{E}^p}{\varepsilon_Y}\right)^N \tag{25}$$

8

via (22).

3.2. Energy boundness analysis

We proceed to obtain the asymptotic nature of $\varepsilon_{ij}^p (r, \theta)$. The finite element solutions presented later in the study consistently reveal that the deviatoric Cauchy stress s_{ij} scales as $r^{-1/2}$. We shall adopt this scaling law for s_{ij} and explore its ramifications. First, note from (23) and (24) that τ_{ijk}, and consequently $\tau_{ijk,k}$, are more singular in r than q_{ij}, as the crack tip is approached. Then, the equilibrium relation (9)b demands that

$$s_{ij} \sim -\tau_{ijk,k} \tag{26}$$

to leading order in r, and consequently τ_{ijk} is of order $r^{1/2}$. This imposes a severe restriction on the form of $\varepsilon_{ij}^p (r, \theta)$. Assume the separation of variables form for ε_{ij}^p in terms of its Cartesian components

$$\varepsilon_{ij}^p = A_{ij} + r^\alpha B_{ij} (\theta) + \cdots \tag{27}$$

where A_{ij} is taken to be independent of θ and the index $\alpha > 0$ remains to be found. First we show that this form satisfies the field equations, and second we justify this choice. Accordingly, the plastic strain gradient reads

$$\varepsilon_{ij,k}^p = \alpha r^{\alpha-1} \bar{B}_{ijk} (\theta) + \cdots \tag{28}$$

where $\bar{B}_{ijk}$ can be expressed in terms of $B_{ij} (\theta)$ and its derivatives with respect to θ. Substitution of (27) and (28) into (4) gives

$$\left(\tilde{E}^p \right)^2 = \frac{4}{3} A_{ij} A_{ij} + \cdots \tag{29}$$

9

along with

$$\frac{\Sigma}{E_p} = \sigma_Y \left(\frac{2}{\sqrt{3}\varepsilon_Y} \right)^{N-1} (A_{ij}A_{ij})^{\frac{N-1}{2}} \qquad (30)$$

Consequently, (26), (24) and (28) give

$$s_{ij} = -\ell^2 \sigma_Y \left(\frac{2}{\sqrt{3}\varepsilon_Y} \right)^{N-1} (A_{pq}A_{pq})^{\frac{N-1}{2}} \left(r^{\alpha-1} \bar{B}_{ijk}(\theta) \right)_{,k} \qquad (31)$$

Upon recalling that s_{ij} scales as $r^{-1/2}$ the above equation implies that $\alpha = 3/2$ for consistency. The above solution reveals that the elastic strain energy density w^E scales as r^{-1} while the plastic strain energy density scales as r^0, upon recalling (21) and (29). Now recall that we require $w \sim J/r$ in order for $w = w^e + w^p$ to give a finite energy release rate J at the crack tip. This is achieved by the elastic field whereas the plastic field is not sufficiently singular in r to give any contribution to the energy release rate. Alternative assumptions can be made for the series expansion of ε_{ij}^p in preference to (27). However, these do not give rise to an equilibrium solution (i.e., Eq. (26) is not satisfied) or they give solutions that are less singular than that of (29). For example, if we assume that the Cartesian components A_{ij} are a function of θ we find that $\varepsilon_{ij,k}^p$ scales as r^{-1} and $\tau_{ijk,k}$ scales as $r^{-(N+1)}$, and the equilibrium relation (29) for s_{ij} is violated. Alternatively, if we take $A_{ij} = 0$ then an equilibrium solution for s_{ij} is obtained provided we take $\alpha = N/(N+1)$. This leads to a higher order term in the series expansion of ε_{ij}^p than that given by the first two terms of (29). Finally, what is the implication of assuming that $\alpha < 0$ in our asymptotic expression (29)? If we were to assume $\alpha < 0$, then the leading order term becomes $r^\alpha B_{ij}(\theta)$. Asymptotic matching of both sides of the equilibrium relation (26) again results in $\alpha = N/(N+1)$, which is inconsistent with the initial assumption that $\alpha < 0$.

In summary, the plastic strain field $\varepsilon_{ij}^p(r, \theta)$ is of the asymptotic form (27) with $\alpha = 3/2$, and the crack tip field for Cauchy stress $\sigma_{ij}(r, \theta)$ and elastic strain $\varepsilon_{ij}^e(r, \theta)$ is given by the usual K-field for a mode I crack.

3.3. Asymptotic crack tip fields

Assume that the leading order terms in ε_{ij}^p, in polar coordinates, are of the form (2)-(3). This choice is consistent with the nature of the symmetry of the solution of a mode I crack tip problem; $\varepsilon_{\theta\theta}^p$ and ε_{rr}^p are even in θ and give rise to $\varepsilon_{yy}^p = A = -\varepsilon_{xx}^p$, $\varepsilon_{xy}^p = 0$ in Cartesian coordinates. The components of the plastic strain gradient and the Laplacian of the plastic strain read

$$\varepsilon_{rr,r}^p = \frac{\partial \varepsilon_{rr}^p}{\partial r} = -\frac{3}{2} r^{1/2} f(\theta) \tag{32}$$

$$\varepsilon_{rr,\theta}^p = \frac{1}{r}\left(\frac{\partial \varepsilon_{rr}^p}{\partial \theta} - 2\varepsilon_{r\theta}^p\right) = -r^{1/2}\left[3f'(\theta) - 2g(\theta)\right] \tag{33}$$

$$\varepsilon_{r\theta,r}^p = \frac{\partial \varepsilon_{r\theta}^p}{\partial r} = \frac{3}{2} r^{1/2} g(\theta) \tag{34}$$

$$\varepsilon_{r\theta,\theta}^p = \frac{1}{r}\left(\frac{\partial \varepsilon_{r\theta}^p}{\partial \theta} + 2\varepsilon_{rr}^p\right) = r^{1/2}\left[g'(\theta) - f(\theta)\right] \tag{35}$$

and,

$$\varepsilon_{rr,kk}^p = \frac{\partial^2 \varepsilon_{rr}^p}{\partial r^2} + \frac{1}{r}\frac{\partial \varepsilon_{rr}^p}{\partial r} + \frac{1}{r^2}\frac{\partial^2 \varepsilon_{rr}^p}{\partial \theta^2} - \frac{2}{r^2}\left(\varepsilon_{rr}^p - \varepsilon_{\theta\theta}^p + 2\frac{\partial \varepsilon_{r\theta}^p}{\partial \theta}\right) \tag{36}$$

$$= r^{-1/2}\left[\frac{7}{4}f(\theta) - f''(\theta) + 4g'(\theta)\right]$$

$$\varepsilon_{r\theta,kk}^p = \frac{\partial^2 \varepsilon_{r\theta}^p}{\partial r^2} + \frac{1}{r}\frac{\partial \varepsilon_{r\theta}^p}{\partial r} + \frac{1}{r^2}\frac{\partial^2 \varepsilon_{r\theta}^p}{\partial \theta^2} + \frac{2}{r^2}\left(\frac{\partial \varepsilon_{rr}^p}{\partial \theta} - \frac{\partial \varepsilon_{\theta\theta}^p}{\partial \theta} - 2\varepsilon_{r\theta}^p\right) \tag{37}$$

$$= r^{-1/2}\left[-\frac{7}{4}g(\theta) + g''(\theta) - 4f'(\theta)\right]$$

11

Now make use of the higher order equilibrium equation (9)b, which asymptotically implies $s_{ij} \approx -\tau_{ijk,k}$. Note that, as $r \to 0$, $\tilde{E}^p$ is of leading order $2A/\sqrt{3}$ and can therefore be treated as a constant. As argued above and demonstrated numerically below, the Cauchy stress is characterized by an inner elastic K-field. Consequently, we make use of the Williams (1957) solution to write

$$s_{rr} = \frac{K_I}{4\sqrt{2\pi r}} \left[\cos\left(\frac{\theta}{2}\right) - \cos\left(\frac{3\theta}{2}\right) \right] \tag{38}$$

$$s_{r\theta} = \frac{K_I}{4\sqrt{2\pi r}} \left[\sin\left(\frac{\theta}{2}\right) + \sin\left(\frac{3\theta}{2}\right) \right] \tag{39}$$

where K_I is the mode I stress intensity factor. The higher order equilibrium follows by suitable substitution of (36)-(39) into (24) and (9)b, to give

$$\frac{K_I \tilde{E}^p}{4\Sigma\sqrt{2\pi}} \left[\cos\left(\frac{\theta}{2}\right) - \cos\left(\frac{3\theta}{2}\right) \right] = -\frac{7}{4} f(\theta) + \frac{\partial^2 f(\theta)}{\partial\theta^2} + 4\frac{\partial g(\theta)}{\partial\theta} \tag{40}$$

$$\frac{K_I \tilde{E}^p}{4\Sigma\sqrt{2\pi}} \left[\sin\left(\frac{\theta}{2}\right) + \sin\left(\frac{3\theta}{2}\right) \right] = \frac{7}{4} g(\theta) - \frac{\partial^2 g(\theta)}{\partial\theta^2} + 4\frac{\partial f(\theta)}{\partial\theta} \tag{41}$$

In addition, the symmetry condition ahead of a mode I crack tip demands that $f(\theta)$ is an even function of θ. Thus, the solution to the system of differential equations is given by

$$f(\theta) = -\frac{K_I \tilde{E}^p}{16\Sigma\sqrt{2\pi}} \left[2\cos\left(\frac{3\theta}{2}\right) + \cos\left(\frac{\theta}{2}\right) + a_1 \cos\left(\frac{\theta}{2}\right) + a_3 \cos\left(\frac{7\theta}{2}\right) \right] \tag{42}$$

$$g(\theta) = -\frac{K_I \tilde{E}^p}{16\Sigma\sqrt{2\pi}} \left[2\sin\left(\frac{3\theta}{2}\right) - \sin\left(\frac{\theta}{2}\right) + a_1 \sin\left(\frac{\theta}{2}\right) + a_3 \sin\left(\frac{7\theta}{2}\right) \right] \tag{43}$$

Now make use of the traction-free boundary conditions $t_{rr} = t_{\theta\theta} = 0$ along the crack flanks ($\theta = \pi$) to obtain a relation between the constants a_1

and a_3. Free boundary conditions on the higher order traction $\tau_{\theta\theta} = 0$ on $\theta = \pi$ implies that

$$f'(\theta) + 2g(\theta) = 0 \quad \text{at} \quad \theta = \pi \tag{44}$$

rendering $a_1 = 7/3 - a_3$. Imposition of vanishing higher order traction $\tau_{r\theta\theta} = 0$ on $\theta = \pi$ is identically satisfied and provides no useful additional information on (a_1, a_3). It follows that numerical analysis is needed to calibrate a_1 and a_3 and obtain a full field solution.

4. Finite element analysis

4.1. Numerical implementation

We make use of the finite element implementation of Martínez-Pañeda et al. (2019) and employ the viscoplastic potential presented by Panteghini and Bardella (2016). The effective stress is related to the gradient-enhanced effective plastic flow rate through a viscoplastic function,

$$\Sigma = \sigma_F(E^p) V(\dot{E}^p) \tag{45}$$

where the current flow stress σ_F depends on the initial yield stress σ_Y and on E^p via a hardening law. We adopt the following isotropic hardening law,

$$\sigma_F = \sigma_Y \left(1 + \frac{E^p}{\varepsilon_Y}\right)^N \tag{46}$$

and assume that the yield strain is $\varepsilon_Y = \sigma_Y/E = 0.003$. The viscoplastic function $V(\dot{E}^p)$ is defined as

$$V(\dot{E}^p) = \begin{cases} \dot{E}^p/(2\dot{\varepsilon}_0) & \text{if } \dot{E}^p/\dot{\varepsilon}_0 \leq 1 \\ 1 - \dot{\varepsilon}_0/\left(2\dot{E}^p\right) & \text{if } \dot{E}^p/\dot{\varepsilon}_0 > 1 \end{cases} \tag{47}$$

13

and the rate-independent limit is achieved by choosing a sufficiently small value of the material parameter $\dot{\varepsilon}_0$. The numerical experiments conducted show that the ratio $\dot{E}^p/\dot{\varepsilon}_0$ is sufficiently high that $V(\dot{E}^p) \approx 1$ in the vicinity of the crack for all remote K values considered.

A mixed finite element scheme is adopted, such that displacements and plastic strains are treated as primary variables, in accordance with the theoretical framework. The non-linear system of equations for a time $t + \Delta t$ is solved iteratively by using the Newton-Raphson method,

$$
\begin{bmatrix} \boldsymbol{u} \\ \boldsymbol{\varepsilon_p} \end{bmatrix}_{t+\Delta t} = \begin{bmatrix} \boldsymbol{u} \\ \boldsymbol{\varepsilon_p} \end{bmatrix}_t - \begin{bmatrix} \boldsymbol{K}_{u,u} & \boldsymbol{K}_{u,\varepsilon^p} \\ \boldsymbol{K}_{\varepsilon^p,u} & \boldsymbol{K}_{\varepsilon^p,\varepsilon^p} \end{bmatrix}_t^{-1} \begin{bmatrix} \boldsymbol{R}_u \\ \boldsymbol{R}_{\varepsilon^p} \end{bmatrix}_t \tag{48}
$$

where the residuals comprise the out-of-balance forces,

$$
\boldsymbol{R}_u^n = \int_V \sigma_{ij} B_{ij}^n \, dV - \int_S T_i N_i^n \, dS \tag{49}
$$

$$
\boldsymbol{R}_{\varepsilon^p}^n = \int_V \left[(q_{ij} - s_{ij}) M_{ij}^n + \tau_{ijk} M_{ij,k}^n \right] dV - \int_S t_{ij} M_{ij,k}^n \, dS \tag{50}
$$

Here, B_{ij} denotes the strain-displacement matrix, and N_i and M_{ij} are the shape functions for the nodal values of displacement and plastic strain components. The components of the consistent stiffness matrix are obtained by differentiating the residuals with respect to the incremental nodal variables. The reader is referred to Martínez-Pañeda et al. (2019) for full details.

4.2. The small scale yielding solution

We make use of the so-called boundary layer formulation to prescribe an outer K-field. Consider a crack with tip at the origin and with the crack plane

along the negative axis of the Cartesian reference frame (x, y). A remote K field is imposed by prescribing the nodal displacements in the outer periphery of the mesh as,

$$u_i = \frac{K}{E} r^{1/2} f_i(\theta, \nu) \tag{51}$$

where ν is Poisson's ratio and the functions $f_i(\theta, \nu)$ are given by

$$f_x = \frac{1+\nu}{\sqrt{2\pi}} (3 - 4\nu - \cos\theta) \cos\left(\frac{\theta}{2}\right) \tag{52}$$

and

$$f_y = \frac{1+\nu}{\sqrt{2\pi}} (3 - 4\nu - \cos\theta) \sin\left(\frac{\theta}{2}\right) \tag{53}$$

Upon exploiting the symmetry about the crack plane, only half of the finite element model is analysed. A mesh sensitivity study reveals that it is adequate to discretise the domain by approximately 5200 plane strain, quadratic, quadrilateral elements.

A representative small scale yielding solution is now presented in Figs. 1 and 2, for the choice $K = 20\sigma_Y \sqrt{\ell}$, $N = 0.1$, $\varepsilon_Y = 0.003$, and $\nu = 0.3$. Conventional J_2 flow theory implies a plastic zone size R_0 of magnitude

$$R_0 = \frac{1}{3\pi} \left(\frac{K}{\sigma_Y}\right)^2 \tag{54}$$

and so the choice $K = 20\sigma_Y \sqrt{\ell}$ implies $R_0 = 42\ell$. Consequently, the plastic zone size is much larger than ℓ for the strain gradient solid also. The plastic zone is plotted in Fig. 1 by showing contours of von Mises plastic strain,

$$\varepsilon_p = \left(\frac{2}{3} \varepsilon_{ij}^p \varepsilon_{ij}^p\right)^{1/2} \tag{55}$$

15

In broad terms, the outer boundary of the plastic zone is given by the contour $\varepsilon_p/\varepsilon_Y = 0.1$. Additional contours for $\varepsilon_p/\varepsilon_Y = 1$ and 3 are included. It is found that $\varepsilon_p/\varepsilon_Y$ attains a plateau value slightly greater than 3 within the contour $\varepsilon_p/\varepsilon_Y = 3$. Consequently, the stress state within this crack tip zone is elastic in nature. This finding is supported by a plot of tensile stress σ_{yy} as a function of r directly ahead of the crack tip $(y = 0)$, see Fig. 2a. The stress component σ_{yy} scales as $r^{-1/2}$ for sufficiently small r. Likewise, the elastic strain component ε_{yy}^e scales as $r^{-1/2}$ for $r/\ell < 1$, see Fig. 2b. Farther from the crack tip $(1 < r/\ell < 10)$ the stress profile σ_{yy} varies with r in the manner of the HRR field, $\sigma_{\theta\theta} \sim r^{-N/(N+1)}$. Beyond the plastic zone $(r/\ell > 10)$ the stress state again converges to the elastic K-field and σ_{yy} scales as $r^{-1/2}$. Thus, both an outer and an inner K field exist. The distributions of $\varepsilon_{yy}^e(r)$ and $\varepsilon_{yy}^p(r)$ are shown in Fig. 2b. Within the elastic zone at the crack tip, and in the outer elastic zone, we have $\varepsilon_{yy}^e \gg \varepsilon_{yy}^p$. In contrast, within the annual region of the crack tip plastic zone, the plastic strains dominate and $\varepsilon_{yy}^p > \varepsilon_{yy}^e$.

The following J-integral argument can be used to show that the magnitude of K for the crack tip elastic zone is identical to that in the outer field. Write the potential energy P of the cracked solid as

$$P(a) = \int_V w \, \mathrm{d}V - \int_{S_T} \left(T_i^\infty u_i + t_{ij}^\infty \varepsilon_{ij}^p \right) \, \mathrm{d}S \tag{56}$$

where $(T_i^\infty, t_{ij}^\infty)$ are the prescribed tractions on a partial boundary S_T, with outward normal n_i. Define J as the energy release rate per unit crack extension, such that

$$J = -\frac{\partial P}{\partial a} \tag{57}$$

for a body of unit thickness in the z direction. Note that

$$\oint \left(wn_x - \sigma_{ij}n_j u_{i,x} - \tau_{ijk}n_k \varepsilon^p_{ij,x} \right) \, \mathrm{d}S \equiv 0 \tag{58}$$

for any closed contour in the solid that excludes the crack tip. Also note that $\sigma_{ij}n_j = 0$ and $\tau_{ijk}n_k = 0$ on the faces of a traction-free crack. Then, an evaluation of J for a contour Γ which encloses the crack tip, starts on the lower crack flank and ends on the upper flank, gives

$$J = \int_\Gamma \left(wn_x - \sigma_{ij}n_j u_{i,x} - \tau_{ijk}n_k \varepsilon^p_{ij,x} \right) \, \mathrm{d}S \tag{59}$$

where the crack lies along the negative x-axis. The proof is straightforward and follows that outlined by (Eshelby, 1956; Rice, 1968) for the conventional deformation theory solid, absent strain gradient effects.

Now evaluate the contour integral J assuming that the stress state (and associated strain energy density w) is given by an elastic K-field. Direct evaluation gives the Irwin relation $EJ/(1 - \nu^2) = K^2$. Upon performing this integration within the crack tip elastic zone of the strain gradient solid, and repeating the evaluation in the outer K-field remote from the crack tip, path independence of J immediately implies that the magnitude of K is the same in the two zones.

4.3. Sensitivity of crack tip fields to strain hardening and material length scale

We proceed to examine the influence of the strain hardening exponent N upon the crack tip stress state, see Fig. 3a. Consistent with the analytical

17

asymptotic analysis of Section 3, the near-tip asymptotic response is independent of the value of N and the three regimes (outer K, elastic-plastic field and inner K) can be readily identified for the three values of N considered. The strain state near the crack tip is shown in the form of the components ε_{yy}^p and ε_{yy} versus r/ℓ in Fig. 3b. The asymptotic value of $\varepsilon_{yy}^p(r \to 0)$ increases slightly with decreasing N. The zone of almost constant ε_{yy}^p near the crack tip is of similar size for $N = 0.1$, 0.2 and 0.3: the size of the elastic core scales with ℓ and is independent of N.

The dependence of $\varepsilon_{yy}^p(r \to 0)$ upon $K/(\sigma_Y \sqrt{\ell})$ is plotted in Fig. 4 for selected values of N. At small $K/(\sigma_Y \sqrt{\ell})$, negligible plasticity exists near the crack tip - the plastic zone vanishes. At larger $K/(\sigma_Y \sqrt{\ell})$ a plastic zone exists and $\varepsilon_{yy}^p(r \to 0)$ increases.

The tensile stress component σ_{yy} is shown as a function of r in Fig. 5 for several values of ℓ/R_0. The reference size of the plastic zone R_0 is given by Irwin's approximation (54). For the strain gradient solid the plastic zone is approximately of size R_0 since $\sigma_{yy}/\sigma_Y \approx 1$ at $r/R_0 = 1$ for all ℓ/R_0 values considered. Also, the inner elastic zone is of extent ℓ to a good approximation. Consequently, the active plastic zone exists between $r \sim \ell$ and $r \sim R_0$.

4.4. Influence on the crack profile and in inhibiting plasticity

Strain gradient plasticity influences the crack tip profile $\delta(r)$ behind the crack tip. Fig. 6 shows the crack opening profile for conventional ($\ell = 0$) and strain gradient plasticity ($\ell = 0.05R_0$), along with the solutions from the HRR field and from linear elasticity. The HRR field crack opening profile is

18

given by

$$\frac{\sigma_Y E \delta}{K^2} = \alpha \left(\frac{r \sigma_Y E}{K^2} \right)^{\frac{N}{N+1}} \tag{60}$$

while the elastic solution reads

$$\frac{\sigma_Y E \delta}{K^2} = \beta \left(\frac{r \sigma_Y E}{K^2} \right)^{\frac{1}{2}} \tag{61}$$

with $\alpha = 0.18$ and $\beta = 0.48$. The finite element results show large differences between conventional and gradient-enhanced plasticity solutions. Strain gradient plasticity sharpens the crack profile to resemble that of an elastic solid.

Now consider the sensitivity of the plastic zone size r_p to the magnitude of $K/(\sigma_Y \sqrt{\ell})$. We have already noted that, when $K/(\sigma_Y \sqrt{\ell})$ is significantly large, the plastic zone size scales with Irwin's approximation R_0 as given by (54). In contrast, when $K/(\sigma_Y \sqrt{\ell})$ is small, we anticipate that the inner elastic core of dimension ℓ dominates the plastic zone; this is shown in Fig. 7. In order to define the size of the plastic zone r_p, a criterion is needed for active yielding. Here, we assume that the plastic zone extends to either the location where $\varepsilon_p/\varepsilon_Y = 0.1$ or 1, see Fig. 7. It is clear from the figure that the plastic zone size r_p scales with K^2/σ_Y^2 in the same manner as the conventional elastic-plastic solid for sufficiently large $K/(\sigma_Y \sqrt{\ell})$. However, at small $K/(\sigma_Y \sqrt{\ell})$, on the order of 5 to 10, the plastic zone vanishes. At an intermediate value of $K/(\sigma_Y \sqrt{\ell})$ the active plastic zone for the strain gradient solid is somewhat larger than that predicted for the conventional solid.

4.5. Regime of J-dominance

The small scale yielding (SSY) approach is valid provided the crack length is much greater than the plastic zone size R_0 at the onset of frac-

19

ture, $a > 7.5\pi R_0$. Thus, on a map with axes a/R_0 and ℓ/R_0 the small scale yielding regime exists for $a/R_0 > 7.5\pi$; this is shown explicitly in Fig. 8. If a/R_0 is in the range $75\pi\varepsilon_Y < a/R_0 < 7.5\pi$, then a J-field exists near the crack tip and the valid loading parameter becomes J instead of K. This regime of J-dominance is also sketched in Fig. 8. We proceed to explore the stress state near the crack tip for the case of J-dominance. To do so we consider a deeply notched beam in three point bending and calculate the tensile stress state ahead of the crack tip.

We follow the ASTM E 1820-01 Standard[2] and model a three point single edge bend specimen, as outlined in Fig. 9. We take advantage of symmetry and model only half of the specimen, with a total of 24000 quadratic quadrilateral plane strain elements. The J-integral is computed following the ASTM E 1820 Standard,

$$J = J^e + J^p \tag{62}$$

with J^e being computed from the remote load and the specimen dimensions and J^p being calculated from the area below the force versus displacement curve. A reference length scale R_0 can be defined from the estimated value of J as

$$R_0 = \frac{1}{3\pi\left(1 - \nu^2\right)} \frac{EJ}{\sigma_Y^2} \tag{63}$$

Crack tip stresses for $a/R_0 = 0.8$ and $W/R_0 = 1.6$ are shown in Fig. 10 for strain gradient plasticity ($\ell/R_0 = 0.1$) and conventional plasticity theory.

---

[2]Standard No. ASTM E 1820-01 "Standard Test Method for Measurement of Fracture Toughness," American Society for Testing and Materials, Philadelphia, PA.

Finite element results reveal that the elastic core is still present for the case of J-dominance; the strain gradient plasticity prediction exhibits the elastic $1/\sqrt{r}$ singularity as $r \to 0$. Thus short cracks, where small scale yielding does not apply, also exhibit an elastic stress state near the crack tip.

5. Conclusions

We examine, numerically and analytically, the crack tip asymptotic response in metallic materials. The solid is characterised by strain gradient plasticity theory, aiming to phenomenologically link scales in fracture mechanics by incorporating the stress elevation due to dislocation hardening. Results reveal that an elastic zone is present in the immediate vicinity of the crack tip. The stresses follow the linear elastic $r^{-1/2}$ singularity and the plastic strains reach a plateau at a distance to the crack tip that scales with the length scale of strain gradient plasticity ℓ. The dominant role of elastic strains in the vicinity of the crack invalidates asymptotic analyses that neglect their contribution to the total strains. The existence of an elastic core is reminiscent of a dislocation free zone, as introduced by Suo et al. (1993).

The emergence of an elastic core has important implications on the onset of plasticity and the crack opening profile. Numerical predictions show that strain gradient plasticity sharpens the crack opening profile to that of an elastic solid. Differences with conventional plasticity are substantial and results suggest that an experimental characterisation of the crack opening profile could be used to infer the value of the length scale parameter. On the other hand, plasticity is precluded if the remote load is not sufficiently large,

21

such that the plastic zone size (as given by, e.g., Irwin's approximation) falls within the elastic core domain.

In addition, we show that the inner elastic regime is also present when the crack is small and an outer elastic K field does not exist. A generalised J-integral is presented for strain gradient solids and the stress fields are computed under J-dominance conditions in a three point single edge bend specimen.

Finally, we note that the material length scale ℓ is on the order of a few microns for most metals. This is roughly the smallest scale at which void nucleation and growth occur, suggesting that the transition to an inner zone dominated by elasticity will have important implications in quasi-cleavage but play a secondary role in ductile fracture.

6. Acknowledgements

References

Aifantis, E. C., 1984. On the Microstructural Origin of Certain Inelastic Models. Journal of Engineering Materials and Technology 106 (4), 326.

Ashby, M. F., 1970. The deformation of plastically non-homogeneous materials. Philosophical Magazine 21 (170), 399–424.

Brinckmann, S., Siegmund, T., 2008. Computations of fatigue crack growth with strain gradient plasticity and an irreversible cohesive zone model. Engineering Fracture Mechanics 75 (8), 2276–2294.

Chen, J. Y., Wei, Y., Huang, Y., Hutchinson, J. W., Hwang, K. C., 1999. The crack tip fields in strain gradient plasticity: the asymptotic and numerical analyses. Engineering Fracture Mechanics 64 (5), 625–648.

Eshelby, J. D., 1956. The Continuum Theory of Lattice Defects. Solid State Physics 3 (C), 79–144.

Fleck, N. A., Hutchinson, J. W., 2001. A reformulation of strain gradient plasticity. Journal of the Mechanics and Physics of Solids 49 (10), 2245–2271.

Fleck, N. A., Muller, G. M., Ashby, M. F., Hutchinson, J. W., 1994. Strain gradient plasticity: Theory and Experiment. Acta Metallurgica et Materialia 42 (2), 475–487.

Fleck, N. A., Willis, J. R., 2009. A mathematical basis for strain-gradient plasticity theory. Part II: Tensorial plastic multiplier. Journal of the Mechanics and Physics of Solids 57 (7), 1045–1057.

Gao, H., Hang, Y., Nix, W. D., Hutchinson, J. W., 1999. Mechanism-based strain gradient plasticity - I. Theory. Journal of the Mechanics and Physics of Solids 47 (6), 1239–1263.

Gudmundson, P., 2004. A unified treatment of strain gradient plasticity. Journal of the Mechanics and Physics of Solids 52 (6), 1379–1406.

Gurtin, M. E., Anand, L., 2005. A theory of strain-gradient plasticity for isotropic, plastically irrotational materials. Part I: Small deformations. International Journal of the Mechanics and Physics of Solids 53, 1624–1649.

Huang, Y., Zhang, L., Guo, T. F., Hwang, K. C., 1997. Mixed mode near-tip fields for cracks in materials with strain-gradient effects. Journal of the Mechanics and Physics of Solids 45 (3), 439–465.

Hutchinson, J. W., 1968. Singular behaviour at the end of a tensile crack in a hardening material. Journal of the Mechanics and Physics of Solids 16 (1), 13–31.

Jiang, H., Huang, Y., Zhuang, Z., Hwang, K. C., 2001. Fracture in mechanism-based strain gradient plasticity. Journal of the Mechanics and Physics of Solids 49 (5), 979–993.

Komaragiri, U., Agnew, S. R., Gangloff, R. P., Begley, M. R., 2008. The role of macroscopic hardening and individual length-scales on crack tip stress elevation from phenomenological strain gradient plasticity. Journal of the Mechanics and Physics of Solids 56 (12), 3527–3540.

Martínez-Pañeda, E., Betegón, C., 2015. Modeling damage and fracture within strain-gradient plasticity. International Journal of Solids and Structures 59, 208–215.

Martínez-Pañeda, E., del Busto, S., Betegón, C., 2017a. Non-local plasticity effects on notch fracture mechanics. Theoretical and Applied Fracture Mechanics 92, 276–287.

Martínez-Pañeda, E., del Busto, S., Niordson, C. F., Betegón, C., 2016a. Strain gradient plasticity modeling of hydrogen diffusion to the crack tip. International Journal of Hydrogen Energy 41 (24), 10265–10274.

Martínez-Pañeda, E., Deshpande, V. S., Niordson, C. F., Fleck, N. A., 2019. The role of plastic strain gradients in the crack growth resistance of metals. Journal of the Mechanics and Physics of Solids (in press).

Martínez-Pañeda, E., Natarajan, S., Bordas, S., 2017b. Gradient plasticity crack tip characterization by means of the extended finite element method. Computational Mechanics 59, 831–842.

Martínez-Pañeda, E., Niordson, C. F., 2016. On fracture in finite strain gradient plasticity. International Journal of Plasticity 80, 154–167.

Martínez-Pañeda, E., Niordson, C. F., Gangloff, R. P., 2016b. Strain gradient plasticity-based modeling of hydrogen environment assisted cracking. Acta Materialia 117, 321–332.

Nielsen, K. L., Niordson, C. F., Hutchinson, J. W., 2012. Strain gradient effects on steady state crack growth in rate-sensitive materials. Engineering Fracture Mechanics 96, 61–71.

Nix, W. D., Gao, H. J., 1998. Indentation size effects in crystalline materials: A law for strain gradient plasticity. Journal of the Mechanics and Physics of Solids 46 (3), 411–425.

Panteghini, A., Bardella, L., 2016. On the Finite Element implementation of higher-order gradient plasticity, with focus on theories based on plastic distortion incompatibility. Computer Methods in Applied Mechanics and Engineering 310, 840–865.

Poole, W. J., Ashby, M. F., Fleck, N. A., 1996. Micro-hardness of annealed and work-hardened copper polycrystals. Scripta Materialia 34 (4), 559–564.

Pribe, J. D., Siegmund, T., Tomar, V., Kruzic, J. J., 2019. Plastic strain gradients and transient fatigue crack growth: a computational study. International Journal of Fatigue 120, 283–293.

Rice, J. R., 1968. Mathematical Analysis in the Mechanics of Fracture. Mathematical Fundamentals 2 (B2), 191–311.

Rice, J. R., Rosengren, G. F., 1968. Plane strain deformation near a crack tip in a power-law hardening material. Journal of the Mechanics and Physics of Solids 16 (1), 1–12.

Stölken, J. S., Evans, A. G., 1998. A microbend test method for measuring the plasticity length scale. Acta Materialia 46 (14), 5109–5115.

Suo, Z., Shih, C. F., Varias, A. G., 1993. A theory for cleavage cracking in the presence of plastic flow. Acta Metallurgica Et Materialia 41 (5), 1551–1557.

Tvergaard, V., Niordson, C. F., 2008. Size effects at a crack-tip interacting with a number of voids. Philosophical Magazine 88 (30-32), 3827–3840.

Wei, Y., Hutchinson, J. W., 1997. Steady-state crack growth and work of fracture for solids characterized by strain gradient plasticity. Journal of the Mechanics and Physics of Solids 45 (8), 1253–1273.

Williams, M. L., 1957. On the stress distribution at the base of a stationary crack. Journal of Applied Mechanics 24, 109–114.

Xia, Z. C., Hutchinson, J. W., 1996. Crack tip fields in strain gradient plasticity. Journal of the Mechanics and Physics of Solids 44 (10), 1621–1648.

List of Figures

Figure 1: Finite element predictions of the different domains surrounding the crack tip in an strain gradient solid at $K = 20\sigma_Y \sqrt{\ell}$. Three regions are identified as a function of the effective von Mises plastic strain ε_p: the outer elastic domain, the plastic zone and the inner elastic core. A scale bar of length 5ℓ is included. Material properties: $N = 0.1$, $\varepsilon_Y = 0.003$, and $\nu = 0.3$.
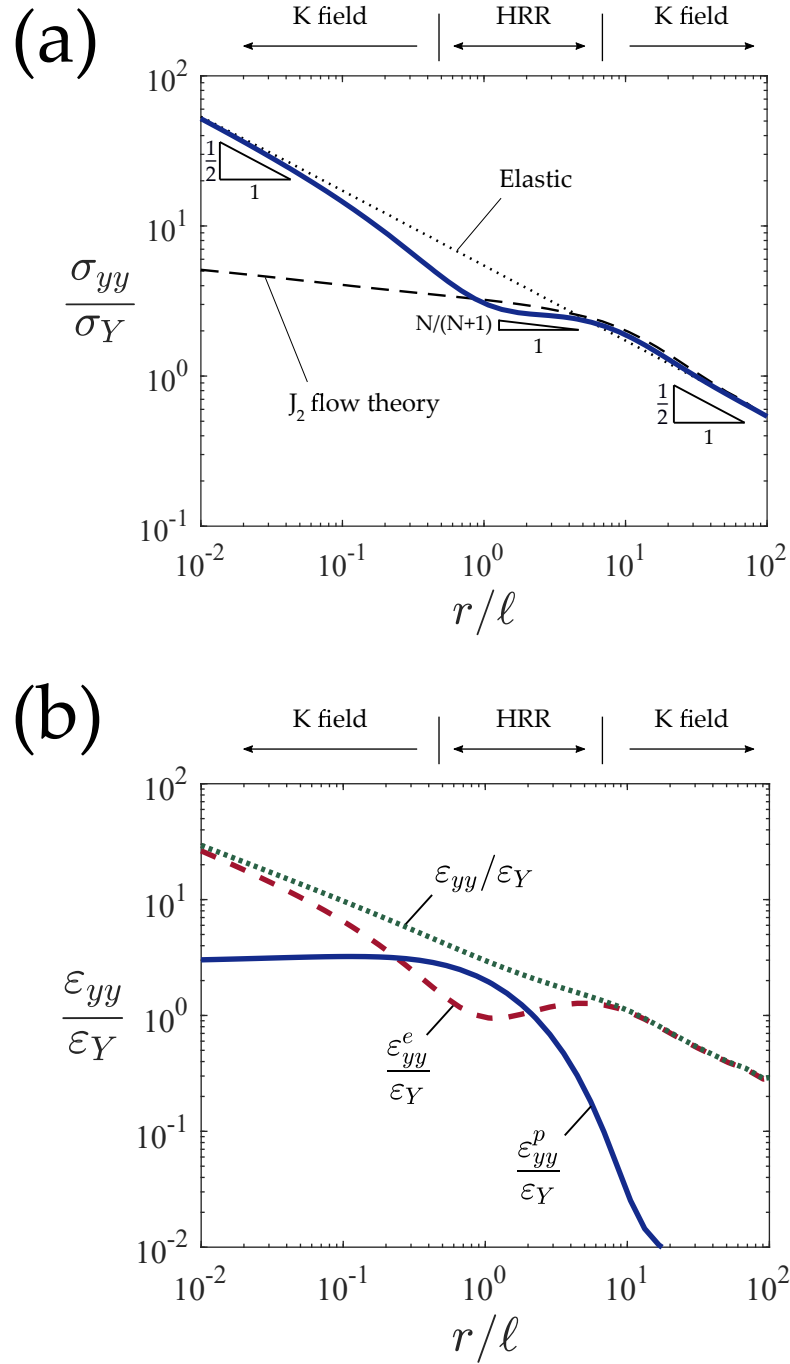
Figure 2: Tensile (a) stress and (b) strain ahead of the crack tip for a strain gradient solid at $K = 20\sigma_Y\sqrt{\ell}$. Material properties: $N = 0.1$, $\varepsilon_Y = 0.003$, and $\nu = 0.3$.
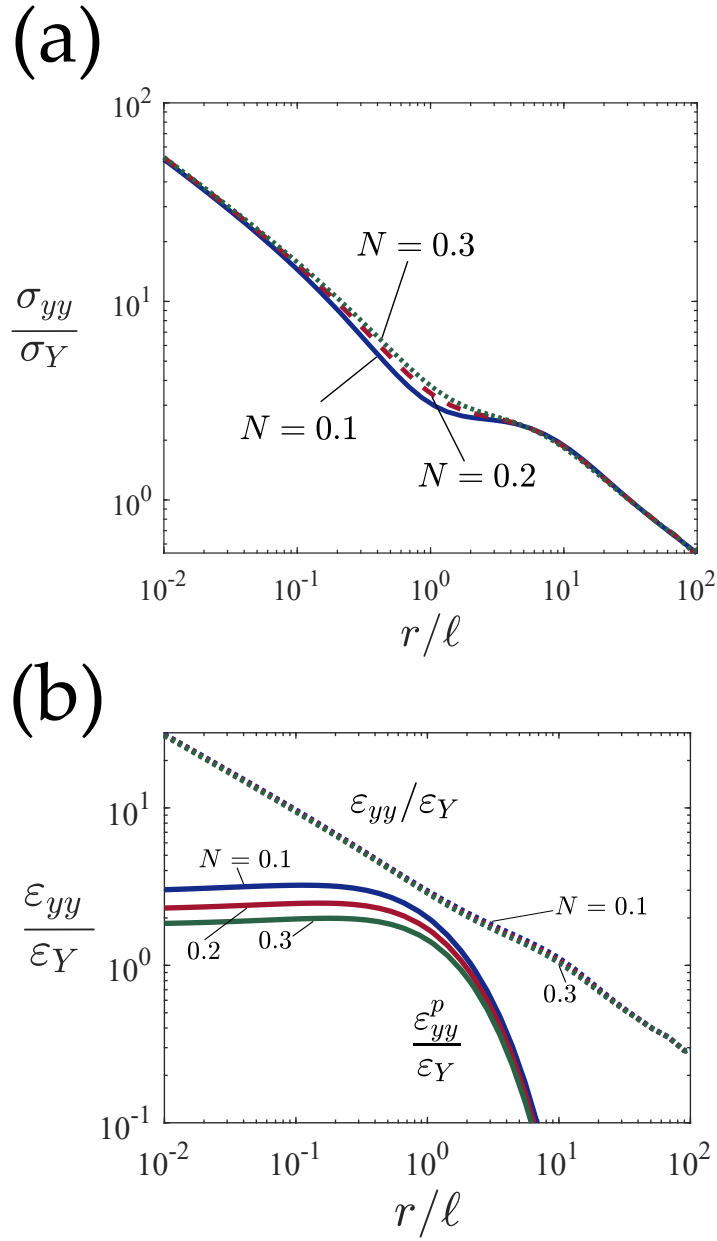
Figure 3: Tensile (a) stress and (b) strain ahead of the crack tip for a strain gradient solid with different values of the strain hardening exponent N at $K = 20\sigma_Y\sqrt{\ell}$. Material properties: $N = 0.1$, $\varepsilon_Y = 0.003$, and $\nu = 0.3$.
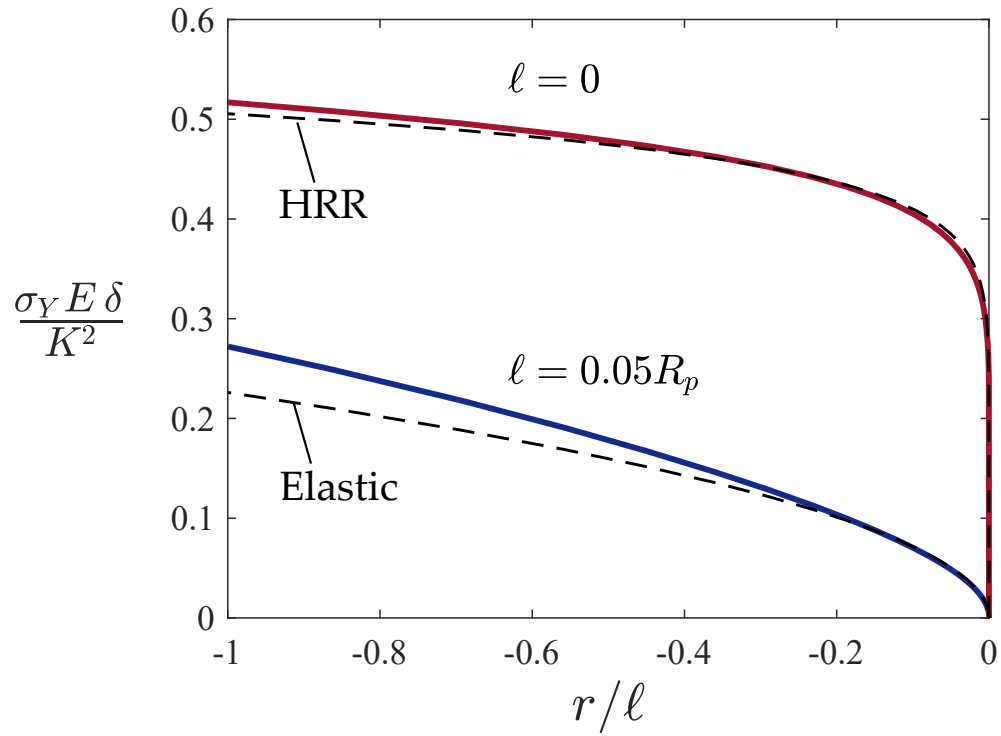
31
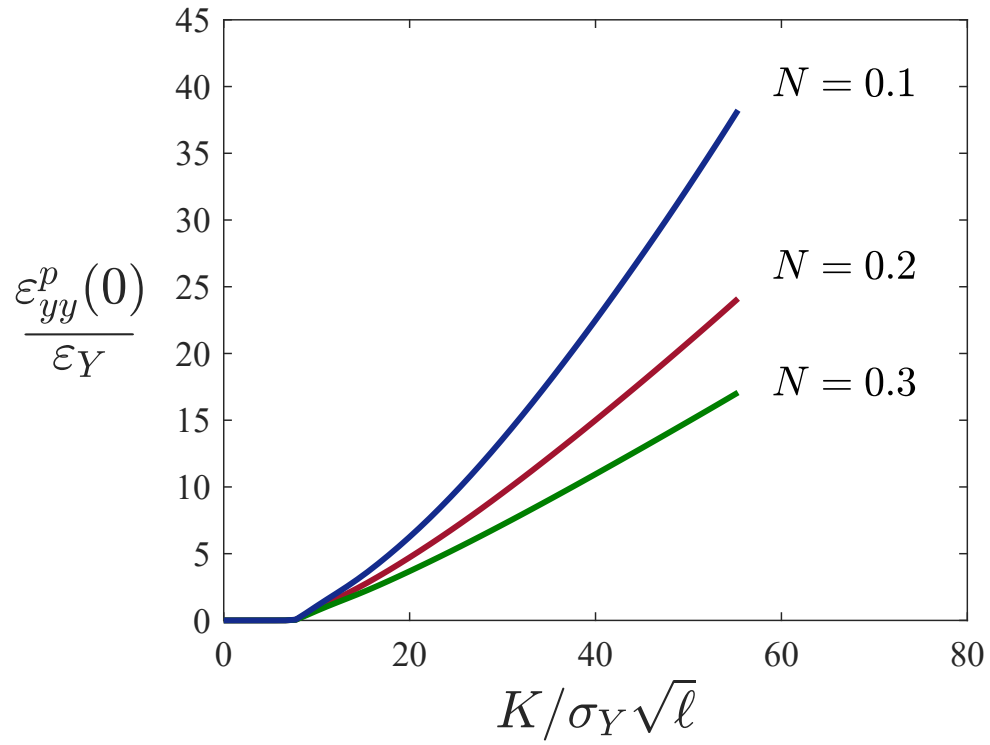
Figure 4: Crack tip plastic strain component ε_{yy}^p as a function of the remote load for different strain hardening exponents. Material properties: $\varepsilon_Y = 0.003$, and $\nu = 0.3$.
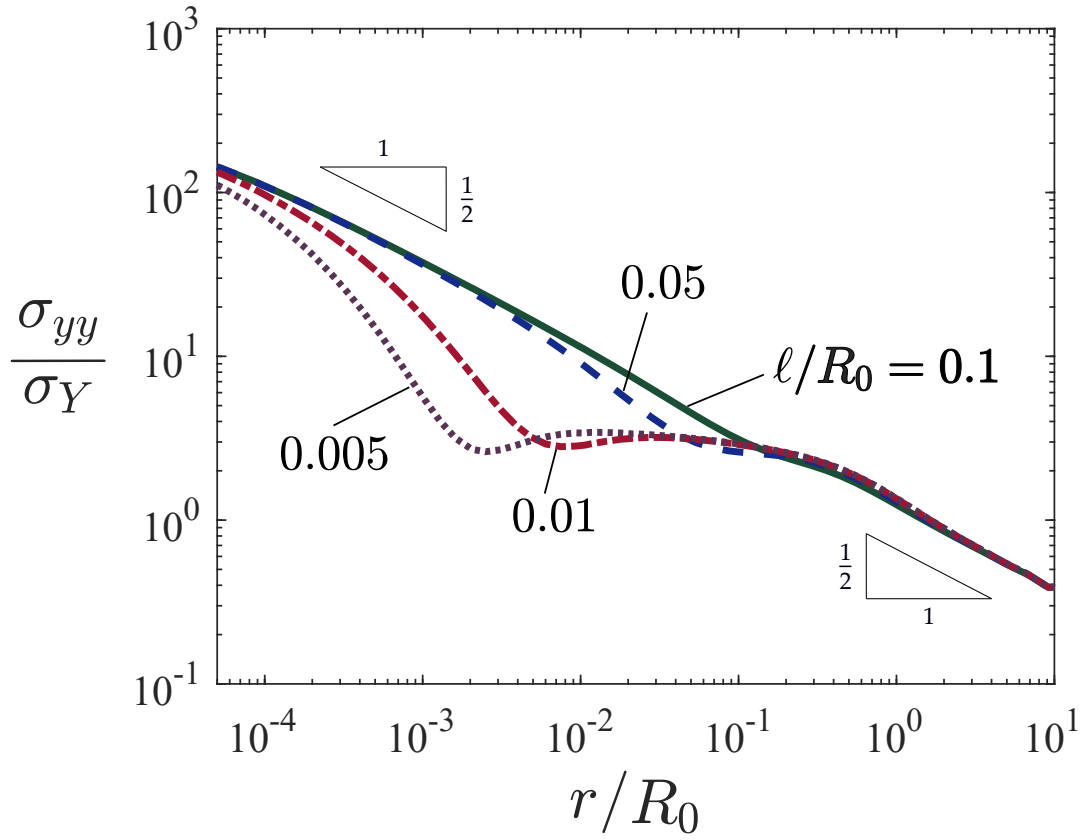
Figure 5: Tensile stress ahead of the crack tip for a strain gradient solid with different values of the length scale parameter at $K = 20\sigma_Y\sqrt{\ell}$. Material properties: $N = 0.1$, $\varepsilon_Y = 0.003$, and $\nu = 0.3$.

Figure 6: Crack opening profile for strain gradient plasticity and conventional plasticity. Material properties: $N = 0.1$, $\varepsilon_Y = 0.003$, and $\nu = 0.3$.
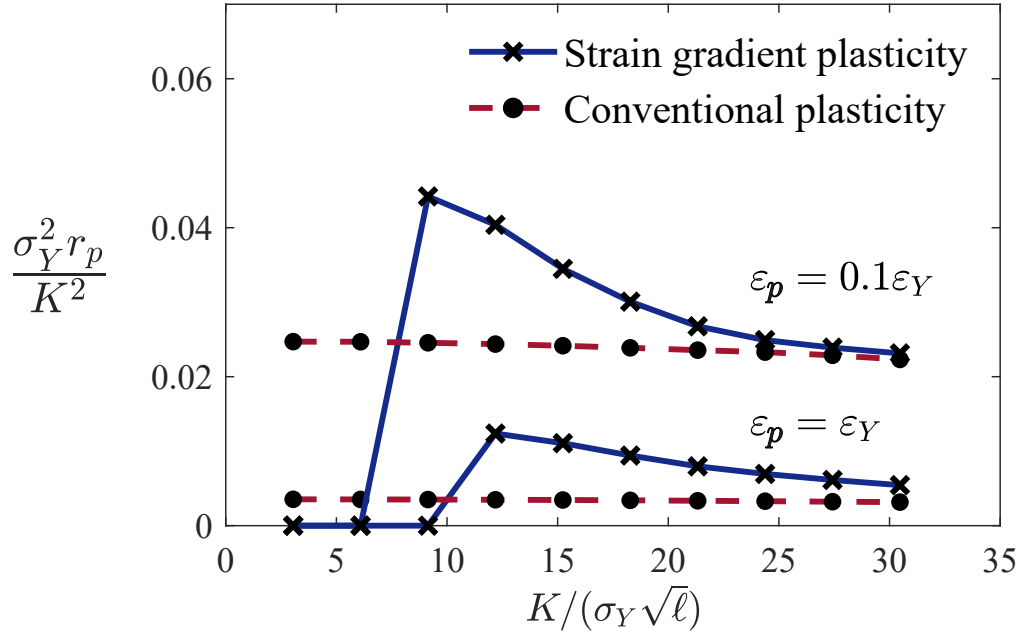
Figure 7: Plastic zone size as a function of the remote load for conventional and strain gradient plasticity. Material properties: $N = 0.1$, $\varepsilon_Y = 0.003$, and $\nu = 0.3$.
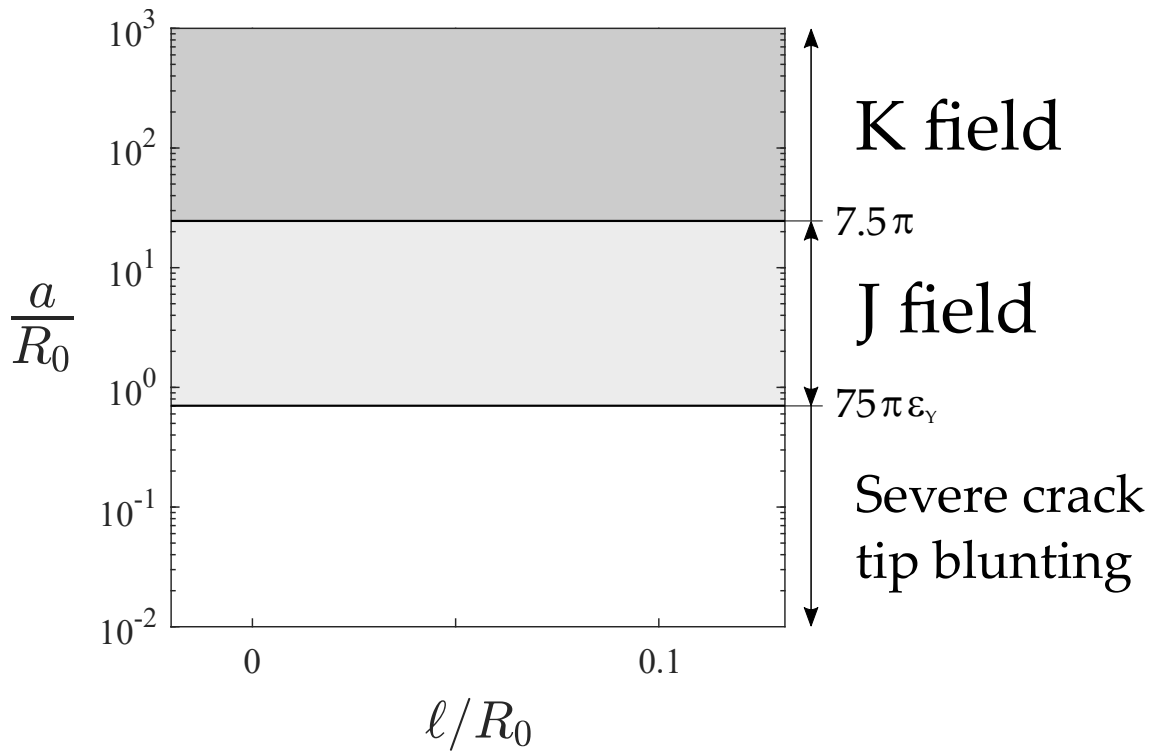
Figure 8: Schematic diagram of the regimes and competing length scales involved in the response ahead of a stationary crack.
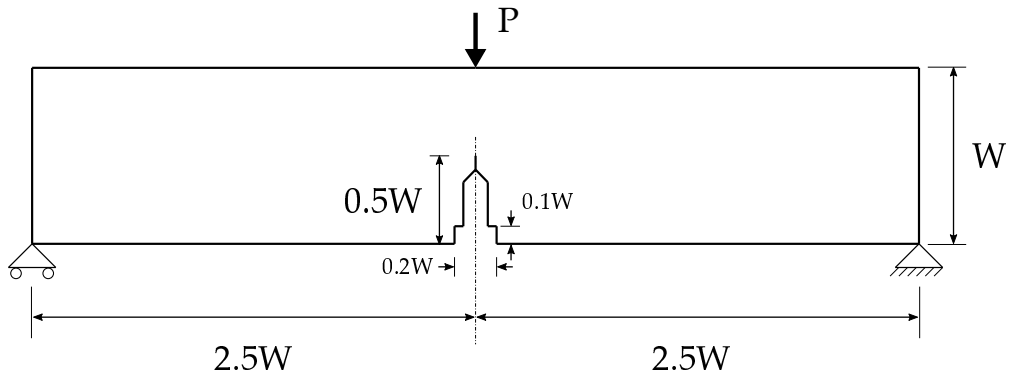
Figure 9: Configuration and dimensions of the three point single edge bend specimen.
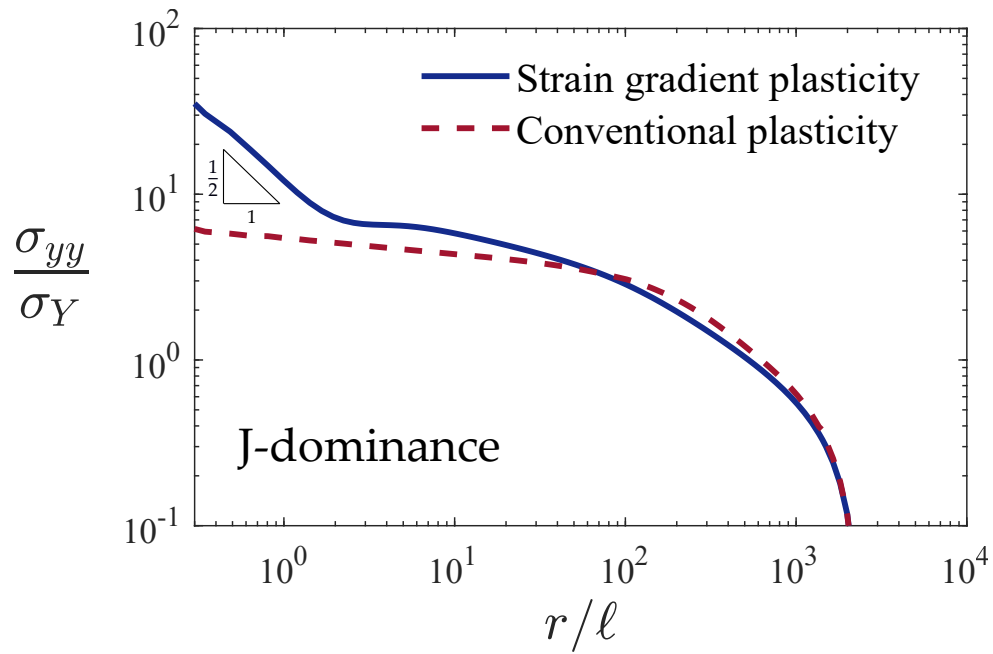
Figure 10: Tensile stresses ahead of the crack tip for conventional and strain gradient ($\ell/R_0 = 0.1$) plasticity under J-dominance conditions. Material properties: $N = 0.1$, $\varepsilon_Y = 0.003$, $\nu = 0.3$, and $a/R_0 = 0.8$.